

Circumsolar irradiance modelling using libRadtran and AERONET data

Cite as: AIP Conference Proceedings **2126**, 190001 (2019); <https://doi.org/10.1063/1.5117698>
Published Online: 26 July 2019

Edgar F. M. Abreu, Paulo Canhoto, and Maria João Costa



View Online



Export Citation

AIP | Conference Proceedings

Get **30% off** all
print proceedings!

Enter Promotion Code **PDF30** at checkout



Circumsolar Irradiance Modelling Using LibRadtran and AERONET Data

Edgar F.M. Abreu^{1, a)}, Paulo Canhoto² Maria João Costa²

¹ MSc. Eng., Instituto de Ciências da Terra. Universidade de Évora, R. Romão Ramalho 59, 7000-671 Évora, Portugal

² Professor – PhD., Departamento de Física, Escola de Ciências e Tecnologia and Instituto de Ciências da Terra. Universidade de Évora. R. Romão Ramalho 59, 7000-671 Évora, Portugal

^{a)} Corresponding author: eabreu@uevora.pt

Abstract. The aperture angle of pyrheliometers is greater than the limit angle of the solar disk, which leads to a contribution of circumsolar radiation to the measurements of direct normal irradiance (DNI). On the other hand, since Concentrating Solar Power (CSP) technologies have, generally, a lower aperture angle with respect to pyrheliometers, it is important to determine the fraction of circumsolar irradiance present in the DNI measurements as well as its angular distribution to provide accurate information for sizing and operation of CSP systems. In this work, the monochromatic circumsolar irradiance (at 675 nm) is modelled using libRadtran and AERONET data at Évora, Portugal for selected cases representing the 1st, 25th, 50th and 75th percentiles of the aerosol optical depth (AOD) measurements distribution at 675 nm and a maximum value of AOD registered during a Saharan dust outbreak in February 2017 in Portugal. The AERONET products used were the columnar values of water vapor content, aerosol optical depth (AOD) and aerosol phase function. Since there are no measurements of circumsolar irradiance at Évora, the assessment of the model output accuracy was done through a comparison of both the modelled DNI from the solar disk only and the DNI including the circumsolar contribution against measurements from a pyrheliometer included in a meteorological station installed at the same location. The mean bias error and the root mean square error were found to be lower for the DNI with the circumsolar contribution, thus validating the modelling approach of circumsolar irradiance.

INTRODUCTION

The measurement of direct normal irradiance (DNI) started in the beginning of the 20th century using instruments (pyrheliometers) that measure not only the direct irradiance from the sun disk but also the irradiance coming from the region close to the sun, known as circumsolar region or solar aureole. The circumsolar radiation is due to the scattering of the sun rays by molecules, aerosols and some cloud types such as cirrus clouds, which transfer the energy from the direct solar beam to a broader cone shaped circumsolar region [1]. Circumsolar radiation (CS) is difficult to measure due to a sharp decrease of intensity between the centre of the solar disk and the outer limit of the field of view of the measuring instruments in the case of a low turbidity atmosphere [2]. In another approach, circumsolar radiation can be determined using modelling techniques such as radiative transfer codes [1] or parametrized models [3]. The DNI is strongly related to the atmosphere transmittance and scattering properties, while the fraction of CS is also related to the scattering angle, decreasing sharply with the increase of the scattering angle.

The sky radiance for a given wavelength and angular position, L_λ , is defined by the angular distance from the centre of the sun ξ and its corresponding azimuth angle φ [2]. Therefore, the angular distance from the centre of the sun ξ and the monochromatic DNI, denoted as $B_{n\lambda}$, are given by, respectively:

$$\xi = \text{acos}(\cos(\theta_S)\cos(\theta) + \sin(\theta_S)\sin(\theta) \cos(\varphi - \varphi_S)) \quad (1)$$

$$B_{n\lambda} = \int_0^{2\pi} \int_0^{\alpha_l} P(\xi, \varphi) L_\lambda(\xi, \varphi) \cos(\xi) \sin(\xi) d\xi d\varphi \quad (2)$$

where θ_s is the solar zenith angle (SZA), φ_s is the solar azimuth angle, θ is the element zenith angle, φ is the element azimuth angle, $P(\xi, \varphi)$ is the penumbra function and α_l is the limit angle of the pyrliometer. The most important angle to determine the field of view of a pyrliometer is the opening half-angle α , which corresponds approximately to the center of the transition between the slope and limit angles ($P(\xi, \varphi) \simeq 0.5$) [5]. If assuming radial symmetry of the sky radiance in the vicinity of the sun position for clear skies, then Eq. (2) can be simplified into [2, 5, 6]:

$$B_{n\lambda} = 2\pi \int_0^{\alpha_l} P(\xi) L_\lambda(\xi) \cos(\xi) \sin(\xi) d\xi \quad (3)$$

Given the small values of ξ in the circumsolar region, Eq. (3) can be further simplified assuming $\cos(\xi) \simeq 1$ and $\sin(\xi) \simeq \xi$ if required. If only the direct radiation from the sun $B_{n\lambda}^{Sun}$ is to be modelled, Eq. (3) must be rewritten with the limit angle of the sun $\delta_{sun} = 0.266^\circ$, replacing the limit angle of the pyrliometer α_l , and the penumbra function is not included provided that δ_{sun} is lower than the slope angle α_s of the instrument (generally true) if modelled data is to be compared with measurements. The penumbra function can be calculated using the geometric characteristics of the pyrliometer, namely the slope and limit angles (α_s and α_l , respectively). The common approach when modelling the radiation received by an instrument is to resort to the geometric penumbra function, used by G. Major [4]. For off-axis angles between 0° and α_s , the penumbra function is equal to 1, while for angles greater than α_l is equal to 0. In the interval $[\alpha_s, \alpha_l]$, the penumbra function is defined by a decreasing function from 1 to 0 given by [4]:

$$P(\xi) = [a^2(\phi - \sin(\phi)) + \mu - \sin(\mu)]/2\pi \quad (4)$$

where

$$\mu = 2\arccos(y_1 - y_2) \quad (4.1)$$

$$\phi = 2\arccos[(y_1 + y_2)/a] \quad (4.2)$$

$$y_1 = (b/2)\tan(\xi) \quad (4.3)$$

$$y_2 = [(a^2 - 1)/2b]/\tan(\xi) \quad (4.4)$$

$$a = (\tan(\alpha_l) + \tan(\alpha_s))/(\tan(\alpha_l) - \tan(\alpha_s)) \quad (4.5)$$

$$b = 2(\tan(\alpha_l) - \tan(\alpha_s)) \quad (4.6)$$

The monochromatic circumsolar radiation $CS_{n\lambda}$ is defined as the part of $B_{n\lambda}$ coming from the annular region defined by two half-angles: the limit angle of the sun δ_s and the limit angle of the pyrliometer α_l , and is given by [1]:

$$CS_{n\lambda}(\delta_{sun}, \alpha_l) = 2\pi \int_{\delta_{sun}}^{\alpha_l} P(\xi) L_\lambda(\xi) \cos(\xi) \sin(\xi) d\xi \quad (5)$$

The modelled DNI for an acceptance function P (penumbra function) and its slope and limit angles can be related to the DNI values from the solar disk only ($B_{n\lambda}^{Sun}$), obtaining the fundamental closure relationship given by:

$$B_{n\lambda} = CS_{n\lambda}(\delta_{sun}, \alpha_l) + B_{n\lambda}^{Sun} \quad (6)$$

The circumsolar ratio (CSR) is then defined as the ratio between $CS_{n\lambda}$ and $B_{n\lambda}$:

$$CSR = \frac{CS_{n\lambda}}{B_{n\lambda}} \quad (7)$$

Information on circumsolar radiation is crucial for the design and operation of CSP systems, because different technologies have different acceptance angles (usually smaller than that of the pyrheliometers that measure DNI) [2], which leads to different amounts of effective radiation being collected by its receivers. In this work, the radiative transfer code libRadtran [7] and products from the AEROSOL ROBOTIC NETWORK (AERONET) [8] were used to estimate the monochromatic DNI and circumsolar radiation at 675 nm ([670 – 680 nm]) under different atmospheric conditions. A monochromatic study is presented here as an assessment study of libRadtran capability in accurately predicting the DNI and circumsolar radiation with specific inputs from AERONET. In the following, the Experimental data and methodology and the Results and discussion sections are presented and, finally, Conclusions are drawn, and future work is discussed.

EXPERIMENTAL DATA AND METHODOLOGY

The experimental data used in this study is obtained from the AERONET station at Évora, located in the Institute of Earth Sciences (IES), University of Évora (38.5678°N, 7.9114°W) and from the meteorological station of IES installed at a few meters from the AERONET station. The AERONET products used were the following: aerosol optical depth (AOD), aerosol single scattering albedo, aerosol phase function, surface albedo and water vapor total column content. Level 1.5 data was used mainly due to scarce sample points in level 2.0 data. The meteorological station of IES measures global solar horizontal, diffuse horizontal and direct normal irradiance, but only DNI measurements obtained through a Kipp & Zonen CHP1 pyrheliometer (First Class instrument according to the ISO 9060) will be used in this work to check the performance of the model.

The simulations in this study were performed for 675 nm and several cases were selected in order to cover different atmospheric conditions. In this way, measurements from the AERONET, which represent the 1st (17/01/2017, 16:02:55), 25th (19/02/2017, 09:47:50), 50th (26/04/2017, 15:34:20) and 75th (07/07/2017, 18:35:45) percentiles of aerosol optical depth (AOD) distribution and the historical maximum (21/02/2017, 08:42:01) occurred during a Saharan dust outbreak were selected. The list of libRadtran inputs is presented in Table 1. The solar radiances were computed using version 1.7 of libRadtran [7] and then the circumsolar irradiance is determined using Eq. (5). The gas absorption parametrization was performed by the adapted code from SBDART. The spectral range used in the simulations was [670 - 680 nm]. Because a spectral range is used, libRadtran requires that all wavelength dependent variables be defined in that spectral range. Therefore, the AOD, single scattering albedo and the Legendre moments of the aerosol phase function were given at 440 nm, 675 nm, and 870 nm.

The extinction coefficient (required by the libRadtran if the aerosol phase function is given) was calculated using the respective monochromatic AOD and considering an atmospheric layer of 10 km. The aerosols were defined using the model proposed by E. Shettle [12], which consists on a rural type aerosol in the boundary layer, background aerosol at 2 km, spring-summer conditions and a visibility of 50 km. The aerosol phase function retrieved from AERONET can be described as the sum of a series of Legendre polynomials and thus it was decomposed in Legendre moments using the *pmom* tool available from libRadtran. The inputs of *pmom* are the measured aerosol phase function and the desired number of Legendre moments. Another tool available with libRadtran is *phase*, which generates the phase function based on the Legendre moments. This tool was used to assess the accuracy of the decomposition of the measured aerosol phase function in Legendre moments. In this way, the measured aerosol phase function was decomposed in 512, 1024, 2048, 4096, 8192, 15000 and 20000 Legendre moments using the *pmom* tool. These moments were then transformed back into phase functions and were compared against the original phase function by means of the root mean square error (RMSE). The RMSE values were calculated considering three different angular ranges, namely, the entire phase function ([0°, 180°]), a forward scattering range ([0°, 5°]) and a backward scattering range ([175°, 180°]), and then averaged for all the phase functions. The RMSE values are presented in Table 2.

TABLE 1. List of the libRadtran inputs.

Input	Origin/Value
Solar spectrum	Gueymard [9]
Spectral range	[670 - 680 nm]
Total column content in water vapor	AERONET
Surface albedo at 440 nm, 675 nm and 870 nm	AERONET
AOD at 440 nm, 675 nm and 870 nm	AERONET
Extinction Coefficient at 440 nm, 675 nm and 870 nm	Derived from AERONET products
Aerosol single scattering albedo at 440 nm, 675 nm and 870 nm	AERONET
Legendre moments of the aerosol phase function at 440 nm, 675 nm and 870 nm	Derived from AERONET products
Mid-latitude summer atmospheric profile	Anderson et al. [10]
Elevation above mean sea level	0.273 km
Sky element zenith and azimuth angles	Defined to achieve ξ up to 6°
Radiative transfer solver	DISORT2 [11]
Number of streams	16

TABLE 2. RMSE values for different number of Legendre moments.

Moments	Mean RMSE		
	[0°, 180°]	[0°, 5°]	[175°, 180°]
512	1.7052	6.9474	8.08x10 ⁻⁴
1024	0.7516	3.0621	7.48x10 ⁻⁴
2048	0.2083	0.8476	6.94x10 ⁻⁴
4096	0.2331	0.9488	6.93x10 ⁻⁴
8192	0.1242	0.5041	6.93x10 ⁻⁴
15000	0.1804	0.7340	6.93x10 ⁻⁴
20000	0.0974	0.3946	6.93x10 ⁻⁴

Since the angle step of the measured aerosol phase function is not uniform in the [0°, 180°] interval, and the *phase* tool requires a specific angle step as input, a spline interpolation of the measured aerosol phase function with a uniform angle step of 0.1° was performed before decomposing it in Legendre moments.

The RMSE decreases with an increasing number of Legendre moments, but not linearly as might be expected. Also, the RMSE is higher for the forward region and lower for the backward scattering region, taking the [0°, 180°] region as reference and regardless the number of moments used. Regarding the complete interval, the higher differences in the mean RMSE are from 512 to 1024 moments and from 1024 to 2048 moments. Although the lower RMSE values are for 20000 moments, the number of chosen moments was 2048 due to computation time issues.

The simulations presented in this work represent a spectral band centered at 675 nm ([670 – 680 nm]), however the experimental DNI is measured at the IES meteorological station in the spectral range of the pyrheliometer, i.e. [280 - 4000 nm]. For this reason, the fraction of solar spectrum correspondent to the 675 nm AERONET band was determined using the ASTM G173-03 reference spectra derived from SMARTS v. 2.9.2 [3]. This fraction is defined as the ratio between the integrated direct and circumsolar irradiance considering the desired wavelength band ([670 - 680 nm]) and the integrated value considering the entire spectrum of measurement ([200 - 4000 nm]).

RESULTS AND DISCUSSION

To exemplify the impact of the atmospheric conditions on the radiance distribution in the circumsolar region, the diffuse solar radiances L_λ at 675 nm was mapped for an angular region between zenith angles of $\theta \pm 6^\circ$ and azimuth angles $\phi \pm 6^\circ$, as shown in Fig.1. The values of the solar zenith angle (SZA), AOD at 675 nm and total column content in water vapor (H2O) used to determine these solar radiances are given in Table 3.

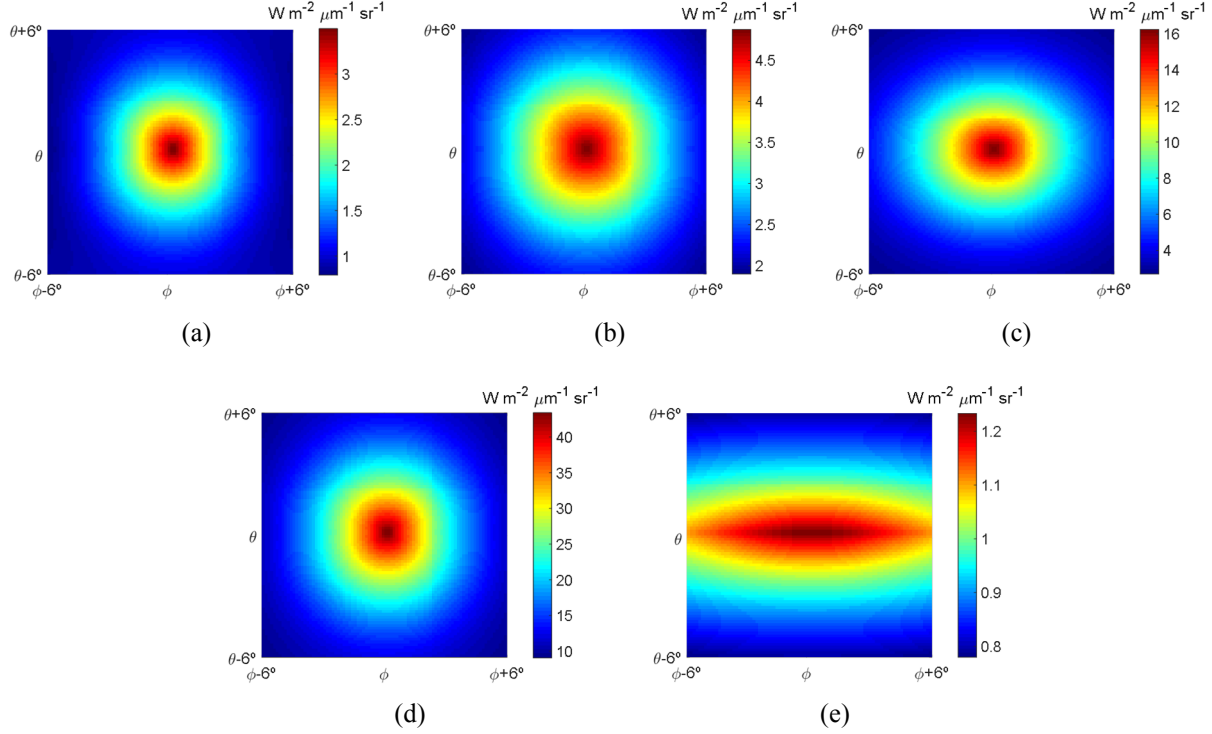


FIGURE 1. Diffuse L_λ at 675 nm at different θ and ϕ angles (details can be found in Table 3).

Regarding the Fig. 1 (a) to (d) and the respective values of AOD and H2O in Table 3, it was found that the intensity of the diffuse radiance L_λ in the circumsolar region ($[\alpha_S, \alpha_L]$) increases with increasing values of AOD. However, the relationship between AOD and L_λ is not linear. In fact, the three parameters presented in Table 3 have a strong impact on the aureole shape. Analyzing Fig. 1 (e), it is possible to verify that that shape was “extended” in the azimuthal direction, due to the high aerosol load resulting from a Saharan dust outbreak and a phenomenon described as horizon brightening, which refers to an enhancement of the radiance intensity near the horizon [13]. The horizon brightening results from the scattering by a large air mass viewed by an observer in that direction [13]. The differences between the several diffuse radiances L_λ presented above can be seen in more detail in Fig. 2, where the normalized azimuthally L_λ profile is shown.

TABLE 3. SZA, AOD and H2O used for the determination of L_λ of Fig. 1.

Subfigure	AOD Percentile	SZA ($^\circ$)	AOD _{675 nm}	H2O (cm^{-1})
(a)	P1	75.559	0.011	13.496
(b)	P25	64.648	0.036	13.215
(c)	P50	50.361	0.060	14.480
(d)	P75	75.969	0.100	32.439
(e)	Max	74.741	1.210	15.956

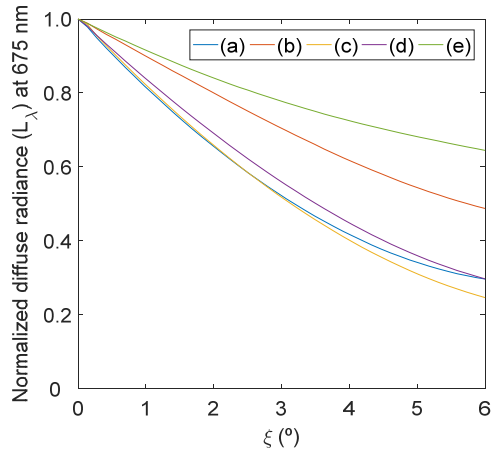


FIGURE 2. Normalized diffuse radiance profile, L_λ ((a) to (e) correspond to the same cases as in Fig.1 and Table 3).

The monochromatic circumsolar radiation $CS_{n\lambda}$ is not measured at Évora. Therefore, the approach presented by Eissa et al. [1] was used to check the accuracy of the modelled $CS_{n\lambda}$ values. In this way, the broadband DNI measurements were multiplied by the fraction corresponding to the considered wavelength interval ($B_{n\lambda}^{exp}$) and compared against the modelled DNI values from the solar disk only ($B_{n\lambda}^{Sun}$) and against the modelled DNI values from the solar disk plus the circumsolar irradiance ($B_{n\lambda}$). Figure 3 presents this comparison together with the mean bias error (MBE) and the root mean square error (RMSE) for each case.

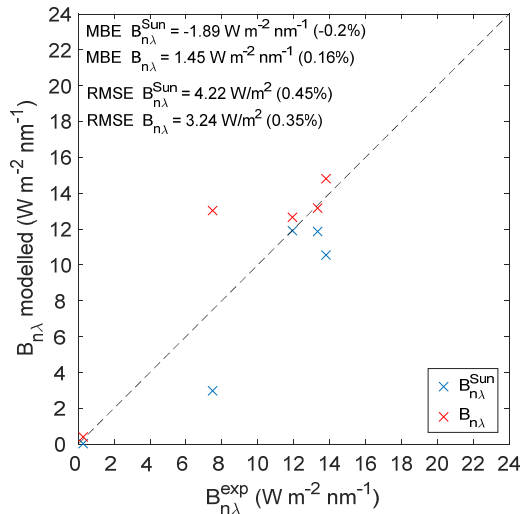


FIGURE 3. Comparison of $B_{n\lambda}^{Sun}$ (blue symbols) and $B_{n\lambda}$ (red symbols) against $B_{n\lambda}^{exp}$.

As expected, the $B_{n\lambda}^{Sun}$ presents a negative bias (-0.20%) when compared to $B_{n\lambda}^{exp}$ because the circumsolar component $CS_{n\lambda}$ is not included in the modelled values while it is measured by the pyrheliometer. On the other hand, the bias of $B_{n\lambda}$ is positive (0.16%), indicating a slight overestimation of the total irradiance measured by the pyrheliometer, although in a lower amplitude if the absolute values of MBE are considered. The RMSE of $B_{n\lambda}^{Sun}$ (0.45%) is higher than the RMSE of $B_{n\lambda}$ (0.35%), indicating that the inclusion of $CS_{n\lambda}$ improves the accuracy of the modelled values. The results obtained in this work could be influenced by the assumptions made in the derivation of Eq. (5), namely the assumption of radial symmetry of the sky radiance in the vicinity of the sun position for clear skies. In real situations, this is not always the case which can have an impact in the results obtained. On the other hand, these results are in agreement with the results presented by Eissa et al. [1] and encourage a more detailed study, using broadband values and a larger number of cases. Regarding the single case

study analysis, the worst performing case study is the case study (d). The overestimation of $B_{n\lambda}$ for this case may be due to the higher value of H₂O, however, a more detailed analysis is needed to better understand this aspect if required. On the other hand, the best results are for cases (a) and (b), which present lower AOD and H₂O.

CONCLUSIONS

In this work, the radiative transfer code libRadtran was used to determine the monochromatic circumsolar radiation for selected cases representing the 1st, 25th, 50th and 75th percentiles of the aerosol optical depth (AOD) measurements distribution at 675 nm and a maximum value of AOD registered during a Saharan dust outbreak in February 2017 in Portugal. The libRadtran inputs were obtained from the AERONET station at Évora and the parameters used in the simulations were the surface albedo, the aerosol single scattering albedo, the total column content in water vapor and the aerosol phase function. Since there are no measurements of the monochromatic circumsolar radiation ($CS_{n\lambda}$) in Évora, the accuracy of the modelled values was found through the comparison of the modelled DNI values for the solar disk only ($B_{n\lambda}^{Sun}$) and the modelled DNI values including the circumsolar radiation ($B_{n\lambda}$) against the measured broadband DNI values from a pyrheliometer downscaled for the same spectral range of simulations ($B_{n\lambda}^{exp}$), located in the same location of the AERONET station. The $B_{n\lambda}^{Sun}$ values presented a MBE of -0.20% and a RMSE of 0.45% while the $B_{n\lambda}$ presented a MBE of 0.16% and a RMSE of 0.35%. These results show that the inclusion of the circumsolar radiation $CS_{n\lambda}$ improves the results obtained from libRadtran, thus validating the $CS_{n\lambda}$ values obtained. These results also encourage to a more detailed study using all the available data from the two stations at Évora as well as the study of the broadband circumsolar radiation, aiming their posterior usage in the design and optimization of Concentrating Solar Power (CSP) plants.

ACKNOWLEDGMENTS

The work was supported by the European Union through the European Regional Development Fund, included in the COMPETE 2020 (Operational Program Competitiveness and Internationalization) through the ICT project (UID/GEO/04683/2013) with the reference POCI-01-0145-FEDER-007690 and also through the DNI-A (ALT20-03-0145-FEDER-000011) project. The authors also acknowledge AERONET / PHOTONS and RIMA networks for the scientific and technical support and Samuel Bárias for maintaining instrumentation used in this work.

REFERENCES

1. Y. Eissa, P. Blanc, H. Ghedira, A. Oumbe, L. Wald, A fast and simple method to estimate the contribution of the circumsolar irradiance to measured broadband beam irradiance under cloud-free conditions in desert environment, *Solar Energy* 163, 497-509 (2018).
2. P. Blanc, B. Espinar, N. Geuder, C. Gueymard, R. Meyer, R. Pitz-Paal, B. Reinhardt, D. Renné, M. Sengupta, L. Wald, S. Wilbert, Direct normal irradiance related definitions and applications: The circumsolar issue, *Solar Energy* 110, 561-577 (2014).
3. C. Gueymard, Parameterized transmittance model for direct beam and circumsolar spectral irradiance, *Solar Energy* 71, 325-346 (2001).
4. G. Major, Circumsolar Correction for Pyrheliometers and Diffusometers, WMO Report 635 (1994).
5. C. Gueymard, Turbidity determination from broadband irradiance measurements: a detailed multi-coefficient approach, *J. Appl. Meteorol.* 37, 414-435 (1998).
6. D. Buie and A.G. Monger, The effect of circumsolar radiation on a solar concentrating system, *Solar Energy* 76, 181-185 (2004).
7. B. Mayer and A. Kylling. Technical note: The libRadtran software package for radiative transfer calculations - description and examples of use, *Atmos. Chem. Phys.* 5, 1855-1877 (2005).
8. B. N. Holben, T.F. Ecken, L. Slutsker, D. Tanre, J.P. Buis, A. Setzer, E. Vermote, J.A. Reagan, Y.J. Kaufman, T. Nakajima, F. Lavenu, I. Jankowiak, A. Smirnov, AERONET – a federated instrument network and data archive for aerosol characterization, *Remote Sens. Environ.* 66, 1-16 (1998).
9. C. Gueymard, The sun's total and spectral irradiance for solar energy applications and solar radiation models, *Solar Energy* 76, 423-453 (2004).

10. G.P. Anderson, S.A. Clough, F.X. Kneizys, J.H. Chetwynd, E.P. Shettle, Atmospheric Constituent Profiles (0-120 km), Air Force Geophys. La., Hanscom Air Force Base, Bedford, Mass., USA Tech. Rep. AFGL-TR-86-0110 (1986).
11. K. Stammes, S.C. Tsay, W. Wiscombe, I. Laszlo, DISORT: a General-Purpose Fortran Program for Discrete-Ordinate-Method Radiative Transfer in Scattering and Emitting Layered Media: Documentation of Methodology, Tech. rep. (2000), Dept. of Physics and Engineering Physics, Stevens Institute of Technology, Hoboken, NJ 07030.
12. E. Shettle, Models of aerosols, clouds and precipitation for atmospheric propagation studies, Atmospheric propagation in the uv, visible, ir and mm-region and related system aspects, AGARD Conference Proceedings, no. 454 (1989).
13. P.C. Jain, Modelling of the diffuse radiation in environment conscious architecture: the problem and its management, [Solar & Wind Technology](#) 6, 493-500 (1989).